

See discussions, stats, and author profiles for this publication at: <https://www.researchgate.net/publication/50305428>

Molecular Dynamic Simulation of Wild Type and Mutants of the Polymorphic Amyloid NNQNTF Segments of Elk Prion: Structural Stability and Thermodynamic of Association

ARTICLE *in* BIOPOLYMERS · SEPTEMBER 2011

Impact Factor: 2.39 · DOI: 10.1002/bip.21611 · Source: PubMed

CITATIONS

19

READS

41

2 AUTHORS:



Workalemahu M Berhanu

University of Central Florida

37 PUBLICATIONS 290 CITATIONS

[SEE PROFILE](#)



Artem E. Masunov

University of Central Florida

147 PUBLICATIONS 2,537 CITATIONS

[SEE PROFILE](#)

Molecular Dynamic Simulation of Wild Type and Mutants of the Polymorphic Amyloid NNQNTF Segments of Elk Prion: Structural Stability and Thermodynamic of Association

Workalemahu M. Berhanu,¹ Artëm E. Masunov^{1,2}

¹ NanoScience Technology Center, Department of Chemistry, University of Central Florida, Orlando, FL 32826

² Department of Physics & Florida Solar Energy Center, University of Central Florida, Orlando, FL 32826

Received 14 October 2010; revised 2 February 2011; accepted 5 February 2011

Published online 7 March 2011 in Wiley Online Library (wileyonlinelibrary.com). DOI 10.1002/bip.21611

ABSTRACT:

A hexapeptide with amino acid sequence NNQNTF from the elk prion protein forms amyloid fibrils. Here we use molecular dynamic simulations of the oligomers and their single point glycine mutants to study their stability. In an effort to probe the structural stability and association thermodynamic in a realistic environment, all wildtype of NNQNTF polymorphic forms with different size and their corresponding double layer 5 strands single point glycine mutants were subjected to a total of 500 ns of explicit-solvent molecular dynamics (MD) simulation. Our results show that the structural stability of the NNQNTF oligomers increases with increasing the number of β -strands for double layers. Our results also demonstrated that hydrophobic interaction is the principle driving force to stabilize the adjacent β -strands while the steric zipper is responsible for holding the neighboring β -sheet layers together. We used MM-PBSA approach free energy calculations to determine the role of nonpolar effects, electrostatics and entropy in binding. Nonpolar effects remained consistently more favorable in wild type and mutants reinforcing the importance of

hydrophobic effects in protein-protein binding. While entropy systematically opposed binding in all cases, there was no observed trend in the entropy difference between wildtype and glycine mutant. Free energy decomposition shows residues situated at the interface were found to make favorable contributions to the peptide-peptide association. The study of the wild type and mutants in an explicit solvent may provide valuable insight for amyloid aggregation inhibitor design efforts. © 2011 Wiley Periodicals, Inc. *Biopolymers* 95: 573–590, 2011.

Keywords: amyloid fibril; amyloid polymorphism; molecular dynamic simulation; β sheet; aggregation; oligomer; steric zipper; molecular dynamic simulations; cross- β structure; binding free energy; MM-PBSA; RMSF; RMSD; elk prion segment of NNQNTF

This article was originally published online as an accepted preprint. The “Published Online” date corresponds to the preprint version. You can request a copy of the preprint by emailing the *Biopolymers* editorial office at biopolymers@wiley.com

INTRODUCTION

Amyloid aggregation involves the association of peptides into supramolecular complexes. The aggregates are typically highly ordered, and *in vivo* they are deposited on tissues in the body. Amyloid fibrils are hallmarks of several neurodegenerative diseases including Alzheimer's, Parkinson's, and prion diseases.¹ The

Additional Supporting Information may be found in the online version of this article.

Correspondence to: Artëm E. Masunov; e-mail: amasunov@mail.ucf.edu

Contract grant sponsor: National Science Foundation

Contract grant number: CCF/CHE0832622

© 2011 Wiley Periodicals, Inc.

atomic resolution structures of several amyloid peptides have been recently determined using x-ray diffraction, electron microscopy, atomic force microscopy, solid state NMR, and computational methods.^{2–4} These atomic resolution structures make it possible to investigate the mechanism of amyloid formation by molecular modeling methods and directly compare the modeling with experimental results. Unlike other protein quaternary structures, amyloid fibrils share a sequence independent structural motif known as the cross β -spine; individual strands from constituent proteins form a β -sheet that runs perpendicular to the fibril axis.² The x-ray diffraction pattern of amyloid fibrils reveals two main characteristic reflections at 4.7 Å (termed main chain spacing) and a broader reflection at 8–12 Å (termed side chain spacing). The main chain spacing measures the distance between two hydrogen bonded β -strands within the same β -sheets forming continuous β -sheets. The sharpness of this (4.7 Å) reflection indicates the low variability and high repetition of the underlying molecular unit along the fibril axis. Its conservation for fibrils formed from different polypeptide sequences reflects the fact that all amyloid fibrils encompass the polypeptide main chain in the same basic molecular arrangement.² In contrast, the side chain spacing was shown to vary significantly for different amyloid fibrils. Spacing between 8.8 and 14.6 Å were observed.⁵ This spacing measures the packing distance between two juxtaposed β -sheets. It depends substantially on the sequence of the amino acid side chains that protrude outward from the cross β -sheets. Hence, this variability reflects the differences of the polypeptide sequences constructing the fibril structure. Taken together, x-ray diffraction shows that the structure of amyloid fibrils is highly conserved along the fibril axis, but variable in the plane of the fibril cross-section.⁵ With these basic features unchanged, the amyloid polymorphism derives from the way the β -strands associate into fibrils. There are three major structural features that may decide the overall amyloid fibril morphologies: (1) differences in backbone orientation, (2) differences in backbone conformation, and (3) differences in the way in which the oligomers, with almost identical structure, associate. The combination of these three factors can give rise to an enormous variation in conformational detail and, consequently, in seed oligomer and fibril morphology.⁶

Eisenberg and co-workers^{2,7,8} have determined more than 20 fibril-like structures of segments from proteins known to fibrillize by x ray microcrystallography. Among these structures seven have been crystallized in two different crystalline forms resulting in different interactions between the peptides (VQIVYK, NVGSNTY, SSTNVG, NNQQ, MVGGVV, GNNQQNY, and NNQNTF). The structures consist of pairs of tightly packed, highly complementary β -sheets,^{2,8} which

are termed “steric zippers.” Hydrogen bonds hold each sheet together and van der Waals interactions bind the two sheets into the zipper spine.^{2,9} Each steric zipper is formed from identical short segments of protein molecules. In actual fibrils and microcrystals, there are tens of thousands of layers. Each strand forms backbone hydrogen bonds to strands above and below it. Polymorphic structures are common among steric zippers. It has been suggested that polymorphism is possible if there are multiple filament structures with similar thermodynamic stability.¹⁰ It is unclear whether similar stability between multiple possible filament structures is a requirement for polymorphism or whether a filament structure can be chosen by a purely kinetic mechanism even if it is not the most stable one. It thus appears that, although amyloid fibrillogenesis is largely a sequence independent phenomenon, for a given peptide sequence, the choice of a specific steric zipper pattern involves intricate interactions between amino acid side chains as well as backbone hydrogen bonds.¹¹

Polymorphism is found in various amyloid fibrils formed by A β , prion, glucagon, and amylin and is influenced by the environment in which the fibrillogenesis occurs. The polymorphic nature of A β peptide fibrils has been suggested to alter their pathogenic action. Polymorphism of amyloids leads to difference in terms of protofilament backbone regions, secondary structure, chromophore alignment along the fibril axis, and fibril superstructure.¹² While the selection of the filament structure depends on the growth condition, which can be purely mechanical agitation, once a stable filament is formed, it continues to grow, keeping the atomistic order even if the growth condition changes. While these experiments are essential for describing supramolecular structures of amyloid fibrils, a fundamental question remains regarding how these structures are formed. Knowledge of the assembly pathway and the structural properties of these fibrils would be useful for developing therapeutic strategies against amyloidoses as well as for developing biomaterials based on peptide self-assembly into β -sheet fibrils. Computer simulations have played an important role in addressing these questions.

Recently, MD simulations had been used to provide an insight into the characteristics of the amyloid aggregates.^{13–17} Masman et al. explored the contributions of the different structural elements of trimeric and pentameric full-length A β (1–42) aggregates in solution to their stability and conformational dynamics.¹⁸ Kent et al. reported that a solvent-exposed hydrophobic patch is believed to be important for aggregation of A β (10–35)¹⁹ Nussinov et al. studied A β 40 elongation and lateral association and the aggregation pathway of β 2-microglobulin amyloid with MD simulations.^{17,20} Garcia et al. investigated the flexibility of the C terminus of

$\text{A}\beta_{42}$ and found the C terminus to be responsible for the higher propensity of this peptide to form amyloid.²¹ DeMarco and Daggett have studied the aggregation process of prion fibril using atomic MD.¹³ Wu et al. have reported the amyloidogenic hexapeptide NFGAIL aggregation.¹⁴ Furthermore, Gnanakaran et al. have investigated the aggregation of simple amyloid β -dimer with replica-exchange MD.¹⁵ Previous theoretical studies have demonstrated the significant role of steric zipper in the structural stability of the GNNQQNY and GGVVIA oligomers stabilized with polar side chain and H-bonding.^{22,23} Park et al.¹⁰ address the structural selection mechanism of different double layer peptides including GNNQQNY, NNQQ, VEALYL, KLVFFAE, and STVIIIE and found that the patterns with the lowest binding free energy correspond to x-ray structures with high accuracy. The main contribution to the binding free energy of the double layer pattern is determined by the van der Waals and hydrophobic forces. These contributions can therefore serve as a quantitative measure of shape complementarity among side chains between the β -sheets. The steric self-complementary interdigitated side chains (known as steric zipper) determine the most stable packing modes. It also makes parallel β -sheets generally preferred over anti-parallel ones. The presence of charged side chains appears to give anti-parallel β -sheets kinetic preference at the early stages of assembly, while the double layer formation is likely to be thermodynamically controlled. Xu et al.²⁴ investigated the β -sheets composed of seven antiparallel decapeptides, representing the 20–29 segment of human Islet amyloid polypeptide (hIAPP). The amyloid nucleus of hIAPP was mimicked with one β -sheet of different initial separation distances between the strands. Multiple all-atom MD simulations with explicit water solvent showed that the assembly occurs not only in the lateral direction but also along the longitudinal direction. This provides a new insight into the assembly pathway at the early stage of fibril elongation. Based on the Poisson-Boltzmann free energy analysis and quasiharmonic configuration entropy estimation, the entropic contribution was found to play an important role in the longitudinal assembly. Moreover, a possible oligomeric state with cyclic form was suggested based on one assembly model found in the simulations. This evidenced the polymorphic nature of the amyloidogenic oligomerization and possible mechanism of its toxicity. The cyclic structures of amyloid oligomers have been reported to be the early intermediates in solution, capable to form ion-channel-like structures in the membrane that could be responsible for pathologic membrane permeability and destabilization of the cellular ionic homeostasis.^{25,26}

Vitagliano et al.²⁷ in their MD simulation characterized the aggregates formed by steric zipper assemblies composed

of a pair of 10-stranded β -sheets of the peptides SSTSAA and VQIVYK that show high fluctuations and significant distortion. The common structure character for these amyloid fibrils implies a common mechanism of pathogenesis.²⁸ This indicates that the study of short peptide aggregation could reveal some common fundamental mechanisms that govern fibril formation in large protein systems.

Prion diseases, also known as transmissible spongiform encephalopathies, include Creutzfeldt-Jakob disease, kuru, fatal familial insomnia, and Gerstmann-Sträussler-Scheinker syndrome in humans; scrapie in sheep; bovine spongiform encephalopathy in cattle; and chronic wasting disease in cervids.²⁹ The prion protein (PrP) is normally present in its native conformation (PrPC). However, in all prion diseases, the protein is present in an abnormal conformation (PrPSc) that accumulates and forms deposits around neurons. A unique feature of prion diseases is that they are transmissible among humans and across species. Evidence suggests that steric zippers are at the core of PrP's pathological form, PrP^{Sc}, giving rise to its appearance as unbranched rods, affinity for amyloid-specific dyes, and diagnostic cross-beta diffraction patterns.^{30,31} In yeast prions, steric zippers are also implied in the mechanism of non-Mendelian inheritance by the obligate conversion of prion to the amyloid state.^{32–35} Previous work has demonstrated that the architecture of amyloid fibrils is determined by specific short segments of the fibril-forming protein which form the "steric zipper" spine of the fibril^{36,2,8,7,37} The structures of amyloid and prion fibrils are different from globular and membrane proteins, in which many segments of the protein contribute to the stability of the structure.³⁸ There is evidence that small steric zippers with complementary structures are related to those in full length proteins and can act as nuclei during the ordered aggregation of full length proteins into amyloid.^{7,8} Prions in the amyloid state act as nuclei seeding the conversion to the amyloid state of the same protein from its soluble monomeric form. The amyloid state can then pass on to progeny cells. Progression and transmission of prion disease in mammals has been suggested to take place in a similar seeding of PrP^C by PrP^{Sc}.^{39,40} Prion amyloid propagation has presented considerable challenges for the development of effective therapeutics to treat prion diseases. Currently, there is no effective therapeutic approach for treating all prion diseases. Future design of therapeutic interventions against the differing amyloid diseases should be primarily targeted at avoiding the appearance of early aggregates in their toxic conformation.⁴¹ One viable approach might be to physically interfere with the aggregation process.⁴⁰

The six-residue NNQNTF segments of elk prion form "steric zippers," between the pairs of interacting β -sheets. In

general, the interfaces between the two sheets in steric zippers are devoid of water; instead they are self-complementary in shape with the side chains of the two sheets tightly interdigitating.² The NNQNTF from elk prion protein forms two facial polymorphic interfaces. Both of these NNQNTF steric zippers packing are found in the same crystal structure. One of them is face to face, with N1, Q3, and T5 of both sheets forming the interdigitated interface while the other one is back-to-back, with side chains N2, N4, and F6 interdigitated (Figure 1).⁸

In this study, we intend to investigate the stability of the hexameric amino acid sequence NNQNTF from the elk prion protein amyloid peptides (NNQNTF polymorphic form I and II) to understand the aggregation mechanisms, the role of individual residues involved in the steric zipper of the oligomer and the thermodynamic of association using MD simulation in explicit water at physiological temperature. We examined the dependence of stability on the position of residue mutation using the tiny β breaker amino acid glycine in solution. In addition, we investigated the most promising potential structural target for further drug design based on the structure-stability information of the wild type and mutants. We utilized the Molecular Mechanics-Poisson-Boltzmann/Surface Area (MM-PBSA) methods for calculating protein-protein binding energies^{42–44} to quantify the driving force underlying the β -sheet association of the wild-type NNQNTF double layers polymorphic forms and their mutants, and we calculated the interaction energy between β -sheets.

MATERIALS AND METHODS

System Setup

The microcrystal structure and coordinate of the parallel β strands of NNQNTF with two different polymorphic forms assembled with two layers of β sheets each comprising of five β -strands has been determined by Eisenberg's group.⁸ The coordinates of polymorphic forms of the pairs of the amyloids peptides NNQNTF were kindly provided by Dr. M. Sawaya.⁸

Molecular Dynamics Simulation

The molecular dynamic (MD) simulation was performed using the AMBER11 package⁴⁵ with an all atom amber99SB force field and explicit TIP3P water models. Each of the amyloid peptides and the corresponding mutants were solvated by explicit water molecules that extends 10 Å from any edge of the octahedral box to the protein atoms. Counter ions were added to the box by randomly replacing water molecules to neutralize the system. Each system was initially energy minimized to remove bad contact by using the conjugate gradient method with the peptide constrained and then to relax the atoms without position constraints. The system was then subjected

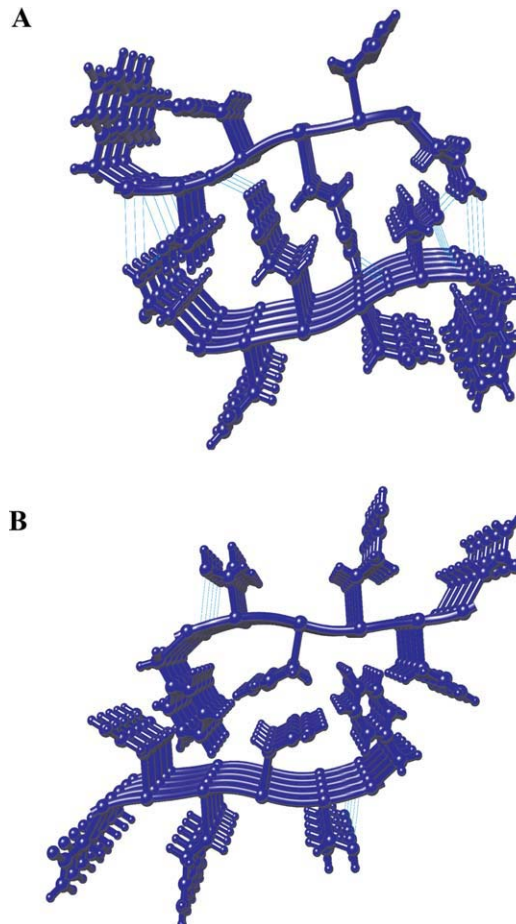


FIGURE 1 The structure of facial polymorphs of NNQNTF segments from elk prion protein. Both NNQNTF steric zippers are found in the same crystal structure, back to back, with side chains N2, N4, and F6 interdigitated (Form I, A) and face to face (right), with N1, Q3, and T5 of both sheets forming the interdigitated interface (Form II, B). Side chain hydrogen bonds are shown in cyan color.

to 50 ps of heating procedure while constraining the backbone atoms of the protein to allow relaxation of water and ions, followed by a 500-ps equilibration run without position constraints on the peptides. Constant pressure (1 atm) and temperature (310 K) on the system was maintained by isotropic Langevin barostat and a Langevin thermostat. Electrostatic interactions were calculated by using the particle mesh Ewald (PME) method.⁴⁶ The cutoff radius for the Lennard-Jones interactions was set to 12 Å. The SHAKE algorithm⁴⁷ was used for bond constraints and the time step will be 2 fs for all simulations. Each system was simulated for 20 ns and the trajectories were saved at 4.0 ps intervals for further analysis. The VMD (visual MD)⁴⁸ program was used for the visualization of trajectories. A hydrogen bond was assigned if the distance between donor D and acceptor A is ≤ 3.5 Å and the angle D-H-A $\geq 120^\circ$.⁴⁹ The MM-PBSA single trajectory approach implemented as script (MMPBSA.py) in AMBER11⁴⁵ was used to calculate the steric zippers binding energy for the non-covalent association between the β -sheets within the double layer. In this approach an assumption is

made that no significant conformational changes occur upon binding, i.e., structural adaptation is negligible and the snapshots for all three species can be obtained from the single trajectory of the complex by separating it into two components. To calculate the binding free energies in the MM-PBSA method, explicit water simulations were used to generate the trajectory followed by the implicit Poisson-Boltzmann/surface area method to calculate solvation energy terms. The binding free energy was calculated using 5000 snapshots over the course of the 20 ns of the MD production trajectories. This approach was previously used by Wu et al.¹⁴ to study the thermodynamics of amyloidogenic peptides.

Mutational Studies

A strategy that has been successful in identifying drug candidates for preventing and reversing amyloid aggregation is the rational development of specific inhibitors based on the use of short peptides targeting the protein region needed for protein–protein interaction. It usually consists of synthesizing short peptides combining a self-recognition motif with a β -sheet disrupting element. The self-recognition domain is typically the region of the protein implicated in early misfolding and protein–protein interaction.⁵⁰ Amyloidogenic sequences tend to lack Pro and Gly, presumably as they are destabilizing in the β -structure.⁵¹ Conservation of glycine and proline residues at structurally strategic positions in β -sandwich proteins appears to serve the purpose of aggregation prevention.⁵² Experiments with *de novo* peptides and proteins as well as with mutated forms of naturally occurring proteins have elucidated features of polypeptide sequence which inhibit aggregation and fibril formation.⁵² Computational mutation of residues involved in the dry steric zipper and between the sheets was preformed to examine the effect of the a single point glycine mutation on sheet to sheet and strand to strand association of the two pairs of short segment amyloid polymorphs of the elk prion.

Computational Mutation

The wild-type five stranded double layer structure was used as the starting structure to generate the single point glycine mutants of NNQNTF forms I and II. The residue substitution at the targeted residues with glycine were carried out using the VMD software.⁴⁸ The wild types were mutated to examine the effect of the side-chain interactions of the amino acids involved in stabilizing the sheet to sheet and strand to strand association of the different amyloid peptide fragments.

RESULTS AND DISCUSSION

Size-Dependent Structural Stability of the Wild-Type Peptide Aggregates

Eight simulations of wild-type NNQNTF form I were conducted for the aggregates built of one (models A1–A4) and two (models A5–A8) antiparallel β -sheets with parallel strands within each sheet (Table I). Another eight wild-type simulations of NNQNTF form II were conducted for the aggregates built of one (models B1–B4) and two (models B5–

B8) antiparallel β -sheets with parallel strands within the sheets (Table II). The conformational change and the conservation of the oligomers were monitored by the time evolution of the backbone root mean square (RMSD) and root mean square fluctuation (RMSF) relative to their initial energy minimized structure as shown in Figures 2 and 3. The RMSDs and RMSF provide useful information on the relative stability of the oligomers and were previously used in stability analyses of amyloid oligomers with β -sheet structure.^{4,53–55}

Root Mean Square Deviation

The conformation change and oligomers' stability of amyloid fibril models and their single point mutants were monitored by the time evaluation of the root mean square deviation (RMSD). The reference structure for calculating backbone RMSD was the energy-minimized structure. As one can see in Figure 2A, for the model systems of the NNQNTF segment of the elk prion peptide polymorph 1 A1 (SH1-ST2) and A2 (SH1-ST3), the RMSDs remained above 20 Å and 10 Å, respectively, for 20 ns, while for A3 (SH1-ST4) and A4 (SH1-ST5) the RMSDs increased to 10 Å, indicating the lower relative instability of the one layer aggregate with the larger number of strands. The larger two-layer model systems of A6 (SH2-ST3), A7 (SH2-ST4), and WT (SH2-ST5) maintained RMSDs, ca. 3.0 Å within 20 ns, indicating relative stability of the structures were compared with the smaller double layer models A5 (SH2-ST2), which showed large fluctuations up to 8.0 Å (Figure 2A). The results of the two-layer models suggested that the structural stability of the NNQNTF polymorph 1 oligomers increases with increasing the numbers of β -strands, and four and five strands are more stable than two and three strands, while for one-layer models there is no clear trend. The same result of the RMSD for polymorph 2 of NNQNTF shows a trend similar to polymorph 1 as shown in Figure 2B. The model systems of B1 (SH1-ST2) and B2 (SH1-ST3) have RMSDs above 20 and below 8, respectively, for 20 ns, while for B3 (SH1-ST4) the RMSDs increased to 18 Å and for B4 (SH1-ST5) it remains below 8 Å, indicating that there is no clear trend. The larger two-layer model systems of A6 (SH2-ST3), A7 (SH2-ST4), and WT (SH2-ST5), maintained RMSDs, ca. 3.0 Å within 20 ns, indicating the relative stability of the structures compared with the smaller double layer models A5 (SH2-ST2), which showed large fluctuations up to 14.0 Å (Figure 2A). Our simulations support the proposal of Nelson et al.³⁶ that the minimal nucleus seed for fibril formation consists of only three to four peptides. Larger oligomers were found not to disassociate quickly due to slow diffusion coefficients. The smaller

Table I Summary of the NNQNTF Oligomeric Models and Simulation Conditions

Model	Systems	Strand/Sheet Organization	Simulation Box Size (Å)	Simulation Time (ns)	T (K)
(A) Simulation condition for NNQNTF polymorph form I					
Wilde type, (NNQNTF)					
A1 (SH1-ST2)	Sheet 1, strands 2	Parallel/antiparallel	48.76 × 48.76 × 48.76	20	310
A2 (SH1-ST3)	Sheet 1, strands 3	Parallel/antiparallel	51.33 × 51.33 × 51.33	20	310
A3 (SH1-ST4)	Sheet 1, strands 4	Parallel/antiparallel	52.16 × 52.16 × 52.16	20	310
A4 (SH1-ST5)	Sheet 1, strands 5	Parallel/antiparallel	54.75 × 54.75 × 54.75	20	310
A5 (SH2-ST2)	Sheet 2, strands 2	Parallel/antiparallel	53.19 × 53.19 × 53.19	20	310
A6 (SH2-ST3)	Sheet 2, strands 3	Parallel/antiparallel	53.58 × 53.58 × 53.58	20	310
A7 (SH2-ST4)	Sheet 2, strands 4	Parallel/antiparallel	56.36 × 56.36 × 56.36	20	310
WT (SH2-ST5)	Sheet 2, strands 5	Parallel/antiparallel	60.50 × 60.50 × 60.50	20	310
Single point mutants					
N1G	Two sheet, five strands (GNQNTF)	Parallel/antiparallel	60.64 × 60.64 × 60.64	20	310
N2G	Two sheet, five strands (NGQNTF)	Parallel/antiparallel	60.40 × 60.40 × 60.40	20	310
Q3G	Two sheet, five strands (NNGNTF)	Parallel/antiparallel	60.74 × 60.74 × 60.74	20	310
N4G	Two sheet, five strands (NNQGTF)	Parallel/antiparallel	60.23 × 60.23 × 60.23	20	310
T5G	Two sheet, five strands (NNQNFG)	Parallel/antiparallel	60.65 × 60.65 × 60.65	20	310
F6G	Two sheet, five strands (NNQNTG)	Parallel/antiparallel	56.30 × 56.30 × 56.30	20	310
(B) Simulation condition for NNQNTF polymorph form II					
Wilde type, (NNQNTF)					
A1 (SH1-ST2)	Sheet 1, strands 2	Parallel/antiparallel	61.28 × 61.28 × 61.28	20	310
A2 (SH1-ST3)	Sheet 1, strands 3	Parallel/antiparallel	61.28 × 61.28 × 61.28	20	310
A3 (SH1-ST4)	Sheet 1, strands 4	Parallel/antiparallel	61.28 × 61.28 × 61.28	20	310
A4 (SH1-ST5)	Sheet 1, strands 5	Parallel/antiparallel	61.28 × 61.28 × 61.28	20	310
A5 (SH2-ST2)	Sheet 2, strands 2	Parallel/antiparallel	57.22 × 57.22 × 57.22	20	310
A6 (SH2-ST3)	Sheet 2, strands 3	Parallel/antiparallel	59.18 × 59.18 × 59.18	20	310
A7 (SH2-ST4)	Sheet 2, strands 4	Parallel/antiparallel	61.23 × 61.23 × 61.23	20	310
WT (SH2-ST5)	Sheet 2, strands 5	Parallel/antiparallel	63.57 × 63.57 × 63.57	20	310
Single point mutants					
N1G	Two sheet, five strands (GNQNTF)	Parallel/antiparallel	63.51 × 63.51 × 63.51	20	310
N2G	Two sheet, five strands (NGQNTF)	Parallel/antiparallel	63.51 × 63.51 × 63.51	20	310
Q3G	Two sheet, five strands (NNGNTF)	Parallel/antiparallel	64.58 × 64.58 × 64.58	20	310
N4G	Two sheet, five strands (NNQGTF)	Parallel/antiparallel	63.60 × 63.60 × 63.60	20	310
T5G	Two sheet, five strands (NNQNFG)	Parallel/antiparallel	63.47 × 63.47 × 63.47	20	310
F6G	Two sheet, five strands (NNQNTG)	Parallel/antiparallel	63.32 × 63.32 × 63.32	20	310

(A) Elk prion fragment (NNQNTF) and six of its mutants. The initial structure is selected from the x-ray structure of the polymorph I. (B) Elk prion fragment (NNQNTF) and six of its mutants. The initial structure is selected from the x-ray structure of the polymorph II.

RMSD values of the polar NNQNTF five stranded double is in a good agreement with the result of Zheng et al.,⁵⁶ who found an RMSD of 2 Å by simulation of a four-stranded double layer GGNNQQNY, which has polar residues on the dry interlayer interface. Our results indicate that the polar dry interface significantly improves stability.

Root Mean Square Fluctuations

The residue-based root mean square fluctuations (RMSF) of the backbones were used to assess the local dynamics and flexibility of each residue for the two polymorphic forms using the PTTRAJ tool in AMBER. Figures 3A and 3B shows

the RMSF profiles of different sizes of the NNQNTF polymorph 1 and 2 oligomers. The RMSF values for all of the wild-type NNQNTF segments of elk prion amyloid peptide models from our simulations for both polymorph forms indicate the flexibility of both N- and C-terminal regions which is consistent with previous experimental and theoretical observations because the flexible regions are unlikely to establish the intermolecular contacts that will stabilize the oligomers.^{56,17} The wild type indicates that all chains have common characteristics of small variation for the central residues (Asn2, Gln3, Asn4, and Thr5). This behavior is particularly apparent for N4, whose side chain is fully buried in the dry interface showing a strong rigidity.

Table II Summary of Structural Analysis of NNQNTF Aggregate Oligomers from MD Trajectories of the Wild-Type and Single Point Glycine Mutant of the Elk Prion Fragment Form X-ray Structure of Polymorph I

System	RMSD	RMSF	$d_{\text{intersheet}}$	$d_{\text{interstrand}}$	# H Bond per Strand*	Secondary Structure	
						β sheet	Turn
2ST-1SH	9.1 ± 8.0	8.9 ± 0.7		11.6 ± 5.9	0.3 ± 0.14	62.4 ± 2.0	37.6 ± 1.4
3ST-1SH	3.8 ± 1.8	2.0 ± 0.9		7.4 ± 1.8	1.0 ± 0.62	73.9 ± 3.0	26.1 ± 2.0
4ST-1SH	4.9 ± 2.2	7.6 ± 1.2		7.6 ± 1.6	1.5 ± 1.0	74.2 ± 3.2	25.8 ± 1.4
5ST-1SH	8.0 ± 5.3	1.7 ± 0.8		8.2 ± 1.9	2.0 ± 1.6	90.2 ± 2.7	9.8 ± 1.4
2ST-2SH	3.8 ± 1.7	3.3 ± 1.4	10.3 ± 1.4	5.9 ± 1.3	0.8 ± 0.7	87.6 ± 4.2	12.4 ± 1.6
3ST-2SH	1.6 ± 0.3	0.8 ± 0.4	8.8 ± 0.5	5.4 ± 0.2	2.7 ± 2.6	90.0 ± 2.9	10.0 ± 1.0
4ST-2SH	1.4 ± 0.2	0.8 ± 0.5	8.5 ± 0.2	5.3 ± 0.2	4.6 ± 3.7	94.7 ± 3.0	5.3 ± 0.6
5ST-2SH	1.6 ± 0.4	1.0 ± 0.5	8.9 ± 0.3	5.4 ± 0.2	5.3 ± 4.1	96.1 ± 3.3	3.9 ± 0.7
N1G	1.6 ± 0.3	0.9 ± 0.7	7.8 ± 0.3	5.2 ± 0.1	4.6 ± 4.8	96.3 ± 3.8	3.7 ± 0.8
N2G	2.1 ± 0.5	0.8 ± 0.6	9.5 ± 0.5	5.4 ± 0.2	4.2 ± 4.8	93.5 ± 4.6	6.5 ± 1.6
Q3G	2.2 ± 0.5	1.6 ± 1.1	6.8 ± 0.2	5.1 ± 0.2	2.1 ± 1.5	94.8 ± 4.9	5.2 ± 1.1
N4G	3.2 ± 1.3	3.4 ± 3.1	9.5 ± 0.7	5.9 ± 0.4	3.4 ± 2.6	90.4 ± 3.4	9.7 ± 1.5
T5G	2.2 ± 0.5	0.8 ± 0.5	8.4 ± 0.3	5.6 ± 0.4	4.6 ± 4.6	93.9 ± 3.7	6.1 ± 1.1
F6G	1.7 ± 0.3	1.6 ± 0.7	9.0 ± 0.3	5.2 ± 0.2	5.3 ± 4.3	96.0 ± 2.7	4.0 ± 0.6

* Average number of hydrogen bonds per strand.

Hydrogen Bond

The analyses of the number of hydrogen bonds of individual residues, averaged from 20 ns simulations for the two polymorphic forms of the elk prion amyloid peptide segments of NNQNTF, are shown in Figures 4A and 4B. The result shows that the average number of hydrogen bonds for the central residues is larger than those for the two end residues for all cases, consistent with the residue-based RMSD results. The larger residue-based RMSDs of the two termini residues are due to the reduction of hydrogen bonds between the peptides. The side chains of the termini residues are more exposed to water and tend to form hydrogen bonds with water molecules rather than peptides. The hydrogen bonds between the end residues of wild type and water molecules are weak and easily break and reform within very short time periods. The two main forces stabilizing proteins are the hydrophobic effect and hydrogen bonding.⁵⁷ Amyloid fibril is characterized by the intra-sheet hydrogen bonds, and hydrogen bonds were found to be necessary to stabilize the main conformational pattern of amyloid fibrils and β -sheets.⁵⁸ Polymorph 1 displays more side chain-side chain hydrogen bonds than polymorph 2 due to the packing polymorphism and due to this polymorph 1 of NNQNTF is more stable than polymorph 2.

Interstrand (d_{strand}) and Intersheet (d_{sheet}) Distances

To examine the structural stability of the wild-type of the NNQNTF polymorphic forms oligomers, we analyzed the interstrand and intersheet. The d_{strand} is calculated by averag-

ing the mass center distance between each residue in one sheet and the respective in-register residue in the adjacent sheet, whereas d_{sheet} is calculated by averaging the mass center distance between sheets.⁵⁶

Interstrand Distance of the Wild Type

The interstrand distance was used to monitor the conservation of the structural stability of the NNQNTF oligomers examined in this study. As shown in Figures 5A and 5B, the d_{strand} of the SH1-ST2 model for the polymorphic forms I and II of NNQNTF raised rapidly around 3 ns and then exhibited remarkable fluctuations for the rest of the simulation, indicating that the SH1-ST2 model is dramatically unstable with the adjacent β -strands being dissociated from each other. Although the SH1-ST3 and SH1-ST4 models are slightly more stable than the SH1-ST2 model, they were considered to be unstable with such high d_{strand} values. The SH1-ST5 model showed a d_{strand} of ca. 10 Å. The result suggests that none of these one-sheet models are able to preserve the structural integrity during the entire simulation. For two-sheet models, it was found that the d_{strand} of the SH2-ST2 model was maintained below 10 and 14 Å for polymorphs 1 and 2, respectively. While the d_{strand} of the SH2-ST3, SH2-ST4, and SH2-ST5 model were ca. 5.0 Å, the smallest stable oligomer is a six-strand species arranged in two layers. The double layer hexamer is the possible nucleus seed for the NNQNTF protofibril. Experimental and MD simulation studies on nucleation had also showed that the trimer for A β (larger than our system) is the minimum nucleus seed,^{59,60}

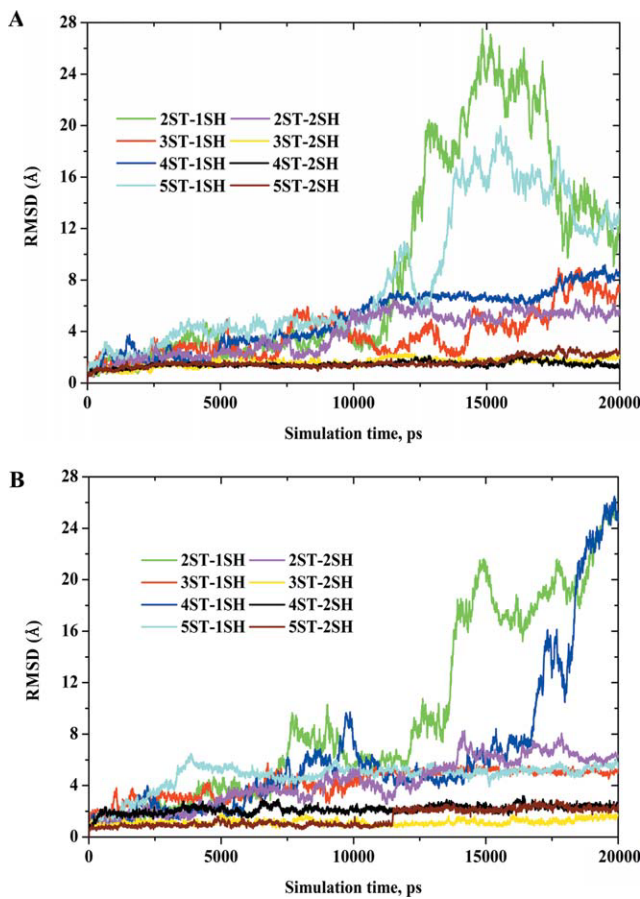


FIGURE 2 RMSDs (RMSD) as a function of the simulation time for the wild-type models of the NNQNTF segment of elk prion. (A) NNQNTF polymorph form 1 and (B) NNQNTF polymorph form 2.

which is in agreement with the results of our simulations.⁵⁶ These results also show that the structural stability of these models increase with increasing the number of the NNQNTF peptide strands, similar to the theoretical study of the amyloid peptide GNNQQNY.⁵⁶ Further, our simulations suggest that the two-sheet models exhibit higher structural stability than the one-sheet models. It can be attributed to the fact that the steric zipper only appears in the two-sheet models.

Intersheet Distance

The intersheet distance for the double layer models of both polymorph forms of the wild-type were found to be within the 8.0–9.0 Å (Figure 6) which is very close to the intersheet distance of 8.50 of the initial intersheet distance for models SH2-ST3 and SH2-ST5. While for model SH2-ST4 it is below 8.50 and 11 for polymorphs 1 and 2, respectively. The result of the intersheet distance for the double layer model SH2-ST2 shows that the d_{sheet} was fluctuating between 8.5 and 12 Å, indicating that the structure lacked stability and the sheets

are moving apart. The intersheet distance for SH2-ST3 and SH2-ST5 suggests that the structures are almost kept stable during the 20 ns simulation.

Effect of Single Point Glycine Mutation Studies

To further monitor the aggregation stability, six mutants were designed for each of the NNQNTF polymorph forms composed of 10 strands (SH2-ST5). The simulation details for each model are summarized in Table I.

RMSD

The RMSD of the five stranded double layer model aggregate of the wild type (WT) and its mutants are shown in Figures

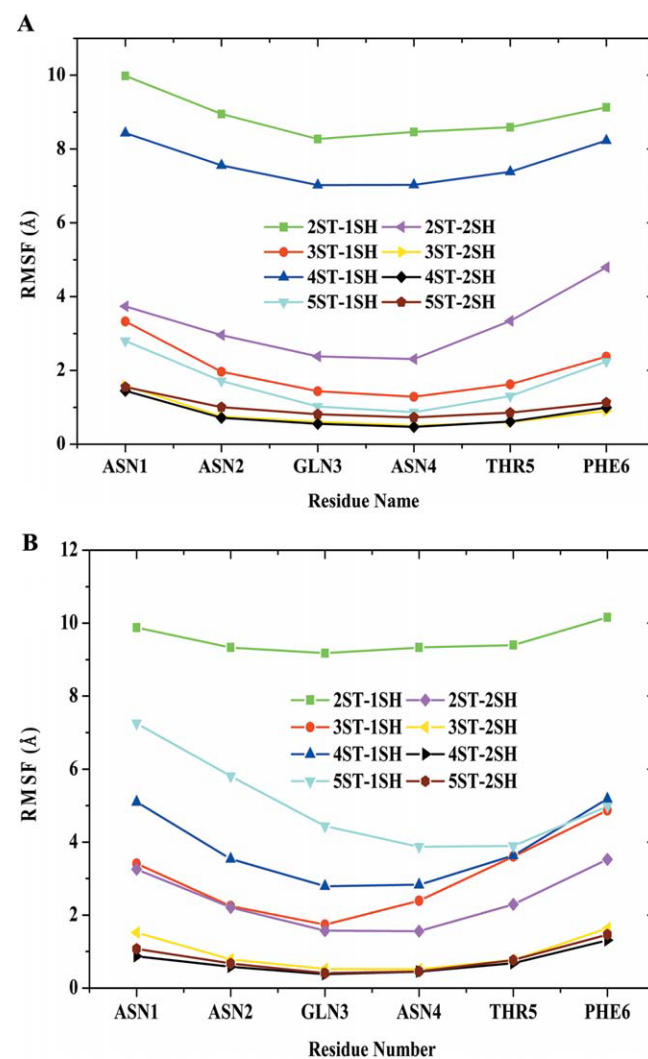


FIGURE 3 Average RMSF of backbone atoms for each residue averaged over the 20 ns of the backbone of wild-type NNQNTF segments of elk prion peptide. (A) Wild-type models of NNQNTF polymorph form I and (B) wild-type models of NNQNTF polymorph form II.

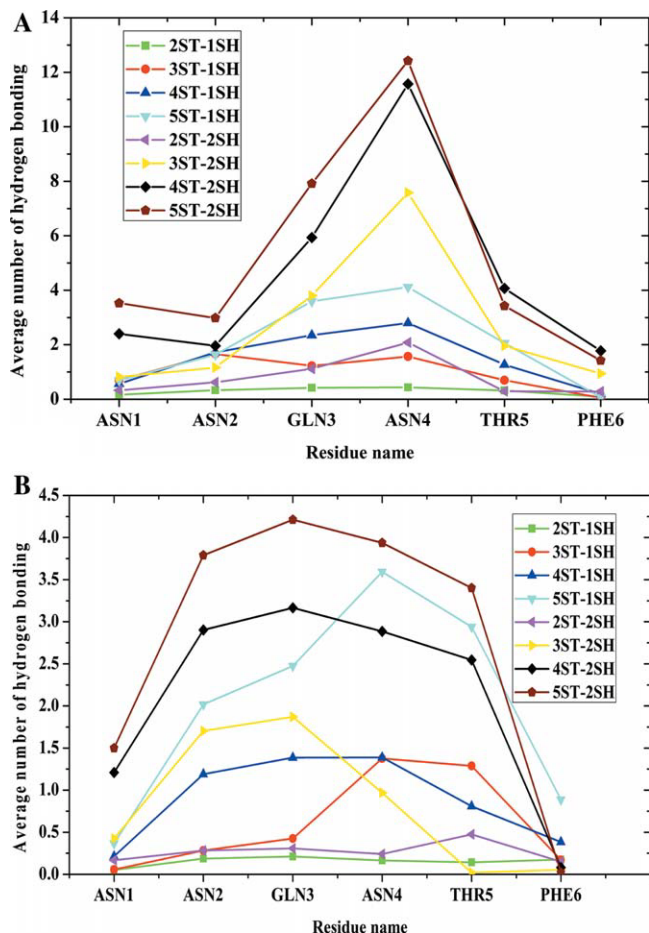


FIGURE 4 Average numbers of hydrogen bonds for individual residues from the simulations of the wild-type models of NNQNTF segment of elk prion with different sizes. (A) Wild-type models of NNQNTF polymorph form I and (B) wild-type models of NNQNTF polymorph form II.

7A and 7B. The result show that N4G of polymorph 1 has an RMSD value of about 5 Å, two times the value of the RMSD of the wild-type, indicating the significant instability of this mutant compared with other mutants. The remaining single point mutants (N1G, N2G, Q3G, T5G, and N6G) have an RMSD in the range of 2.0–2.5 Å, an RMSD value close to that of the wild type. The results indicate the important role of the N4G (whose side chain is fully buried in the dry interface) in stabilizing the oligomers. In the case of NNQNTF polymorph 2, there is significant change in the RMSD values of the mutants. The N4G mutant has an RMSD of 8 Å which is four times higher than the wild type with an RMSD of 2 Å. The mutants that have an RMSD similar to the wild type (such as N1G, Q3G, and F6G) in polymorph 1 have an RMSD value twice the wild type in polymorph 2. This result shows that the residues (Asn1, Gln3, and Phe6) have an important role in stabilizing the packing of polymorph 2. The Phe6 residue in polymorph 2 is involved in the steric zipper.

The RMSD of F6G implies that the Phe6 residue despite being an N terminal has a significant role in keeping the structure stabilized through the π - π interaction of the aromatic side and hydrophobic interaction with the Asn2 side chain of the opposite β -sheet. The mutants N2G and T5G show smaller RMSD and this could likely be due to the smaller size of Gly side, making the mutant N2G and T5G tightly packed. The RMSD result shows that in both polymorphs of NNQNTF a significant change in RMSD was noticed for N4G and in polymorph form 2, besides the mutant N4G, the other three mutants (N1G, Q3G and F6G) have a larger RMSD deviation from the wild type. This could be due to the different packing and interaction of side chains at the double layer interface.

RMSF

The residue-based root mean square fluctuation (RMSF) of the backbones was used to assess the local dynamics and flexibility of each residue using PTTRAJ tool in AMBER. Figures 8A and 8B show the RMSF values of atomic positions by each residue, computed throughout the simulation for wild-type NNQNTF polymorph forms and their corresponding single point glycine mutants. Among the single point mutants, the RMSF values for N4G is much larger for both polymorphs. The next larger RMSF was observed for mutants N1G, Q3G, and F6G for polymorph form 2 of the NNQNTF segment of the elk prion. The mutant F6G in polymorph 2 showed an increase in RMSF despite being an N terminal residue, and this is because the Phe6 is involved in the steric zipper. The smallest fluctuation of the average RMSF in comparison to the wild type was observed for mutant N1G in both polymorph forms which is a C-terminal residue and F6G of polymorph 1.

The RMSF results for the wild type and the mutants indicate that all chains have common characteristics of small variation for the three central residues, whereas large variations for the two end residues, suggesting that the center residues are more rigid than the residues in the termini regions. This is in agreement with the report of Zheng et al.,⁵⁶ and the lowest fluctuation in all cases was observed by residue 4, suggesting a low interchain mobility and a great compactness in this portion. This is a promising target for further drug design based on the structure stability information, such as new potential “amyloid inhibitors” capable of interacting specifically with this portion of the aggregates.

Hydrogen Bonding

The analyses of the number of hydrogen bonds of individual residues, averaged from 20 ns simulations for the wild type and mutants, are shown in Figures 9A and 9B. The result

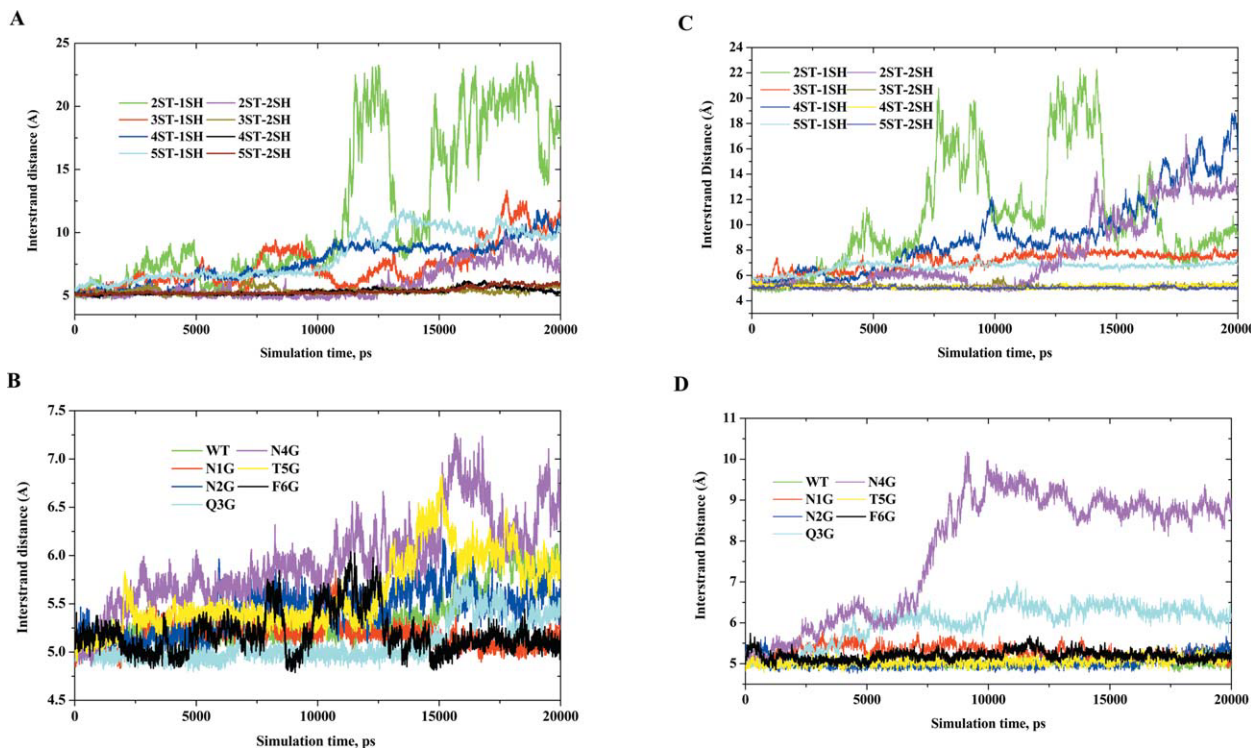


FIGURE 5 The averaged interstrand distances of the wild-type models and mutants during the 20-ns MD simulations. (A) Interstrand distance of wild-type form I NNQNTF. (B) Interstrand distance of wild-type form II NNQNTF. (C) Interstrand distance of wild-type and single point glycine mutants of double layer sheet five strands per sheet models form I NNQNTF. (D) Interstrand distance of wild-type and single point glycine mutants of double layer sheet five strands per sheet models form II NNQNTF.

shows that the average number of hydrogen bonds for the central residues is larger than those for the two end residues for all cases, consistent with the RMSF results. The larger flexibility of the two termini residues were due to the reduction of hydrogen bonds between the peptides. The NNQNTF aggregate oligomer is characterized by the side chain (2Asn-2Asn, 3Gln-3Gln, 4Asn-4Asn and 5Thr-6Phe) for polymorph 2. The polymorph 1, besides the above side chain hydrogen bonds, shows an additional sheet-sheet hydrogen bond, leading to high average hydrogen bonds per residue for polymorph 1 and smaller RMSD for both the wild type and mutants compared to the corresponding system in polymorph 2. The smallest average hydrogen bond per residue for a single mutant was found in mutants for polymorph 2 Q3G, N4G, and F6G, suggesting that Q3, N4, and F6 are key residues for NNQNTF oligomer aggregation. In the case of polymorph 1, replacement of both Q3 and N4 with the β -breaker amino acid Gly resulted in a significant reduction of hydrogen bond in the central residues of the peptide making these mutants structurally unstable. The reduced average hydrogen bonds in the center of aggregation observed for the mutants discussed above indicated that these mutants make the model aggregation oligomer the most unstable which is also evident in the RMSD, RMSF (see above), and intersheet and interstrand distances (see below).

Interstrand Distance

The intersheet distance for both the wild type and most of the mutants were found to be within the 5.5–6.0 Å; which is very close to the intersheet distance of (5.0 Å of the initial intersheet distance of the five-stranded double aggregate oligomer model (Figures 5C and 5D). The result of the intersheet distance between the wild-type and the mutants was found to be very small. This suggests that the strands in the structure are stable during the 20-ns simulation. In the case of the mutants N4G and T5G of polymorph 1, the intersheet distance were within the range of 5.5–7.5 Å indicating the tendency of the sheets to expand in these particular mutants. The interstrand distance for wild-type and the mutants N1G, N2G, T5G, and F6G polymorph form 2 were found to be within the range of 5.0–5.5 Å. While the mutants Q3G and N4G showed an interstrand distance ca. 6.5 and 9.5 Å, respectively, suggesting that the strands of these mutants have a tendency to expand.

Intersheet Distance

The intersheet distance for both the wild type and the mutants are shown in Figures 9C and 9D. The intersheet distance for polymorph form 1 shows that the mutants Q3G and N1G were found to be within the 6.5–7.0 Å and 7.0–8.0

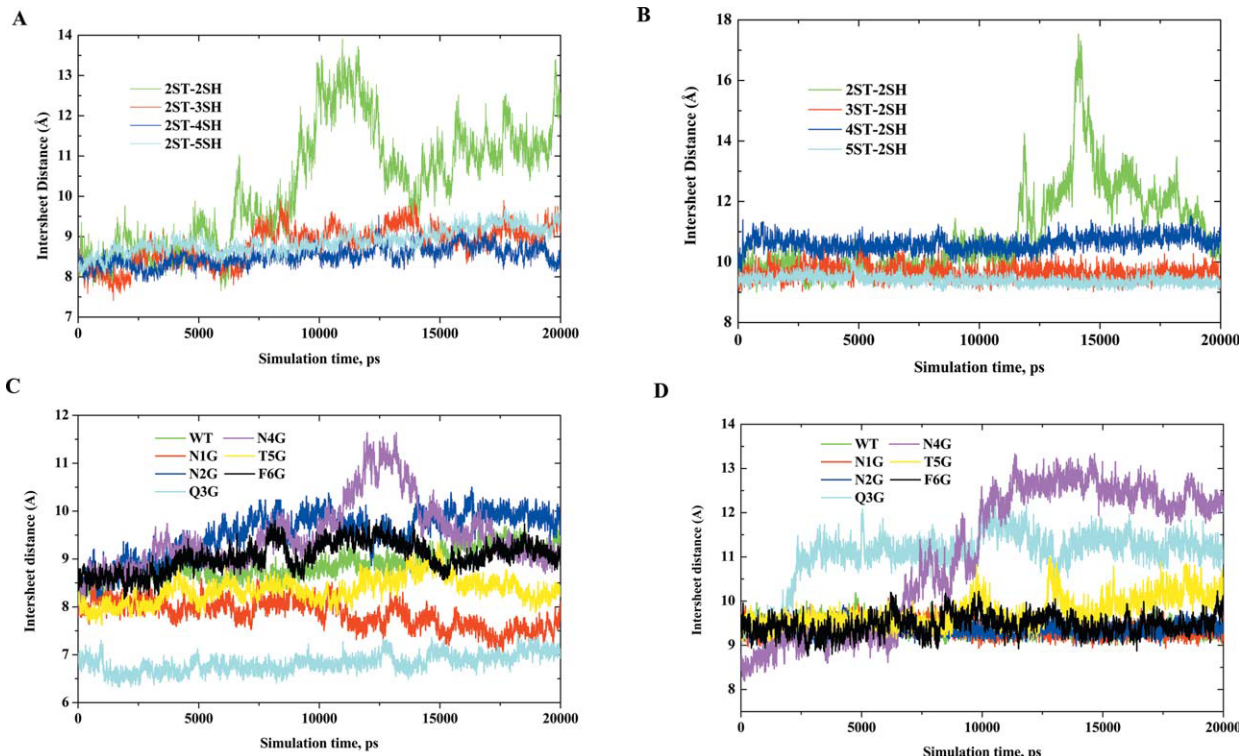


FIGURE 6 The averaged intersheet distances of the wild-type models and mutants during the 20-ns MD simulations. (A) Interstrand distance of wild-type form I NNQNTF. (B) Interstrand distance of wild-type form II NNQNTF. (C) Interstrand distance of wild-type and single point glycine mutants of double layer sheet five strands per sheet models form I NNQNTF. (D) Interstrand distance of wild-type and single point glycine mutants of double layer sheet five strands per sheet models form II NNQNTF.

Å respectively. The intersheet distance for these mutants are found to be smaller than the initial intersheet distance of the wild type (8.5 Å). This is most likely due to the smaller Gly which makes the mutants form a tighter interface. The wild type and the mutant T5G were found to be within the 8.5–9.0 Å, while mutants N2G and F6G have intersheet distance between 8.5 and 10 Å. The intersheet distance for N4G mutant between 8.5 and 11.5 Å show the instability of this mutant and its tendency to expand. The analysis of the interstrand distance measurement shows the significant role of the side chain involved at the peptide-peptide interface to keep the double layers intact.

Snapshots of the final structure from the trajectory of the five-stranded double layers of the studied systems are shown in Figures S1 and S2. As the structure evolves, some of the terminal strands break the β -sheet ordering and twist relative to the remaining strands, although they do not dissociate from the aggregate completely. The degree of this disorder correlates with the RMSD, RMSF, and interstrand and intersheet distances. Among the most disordered structures is the mutant N4G for polymorphs, mutants Q3G and F6G polymorph form 2 and N2G of the polymorph 1. Apparently, the mutated amino acids involved in the steric zippers not only

hold the β -sheets together but also preserve them from disaggregation. Inversely, the complementarity of the amino acid side chains would be essential for the formation of the ordered aggregate. The summary of several geometry analyses of the studied NNQNTF aggregate oligomer and mutants from MD trajectories are given in Tables II and III. The analysis shows that most mutations affect the aggregates' stability, and their stabilities were dependent to a large extent on the position of replaced residues. The smaller aggregate of the wild-type show smaller hydrogen bond per strand and secondary structure content due to their increased flexibility and steric zipper opening.

Sheet-to-Sheet Binding Energy

To further quantify the driving force underlying the β -sheet association of the wild-type NNQNTF segment of elk prion five-stranded double layers polymorph and their mutants, we calculated the interaction energy between β -sheets. For double-layered NNQNTF-sheets, NNQNTF trajectories were first extracted from explicit MD trajectories by excluding water molecules. The solvation energies of double-layered elk prion NNQNTF-sheets and each single-layered elk prion NNQNTF-sheet were calculated using the MM-PBSA (Mo-

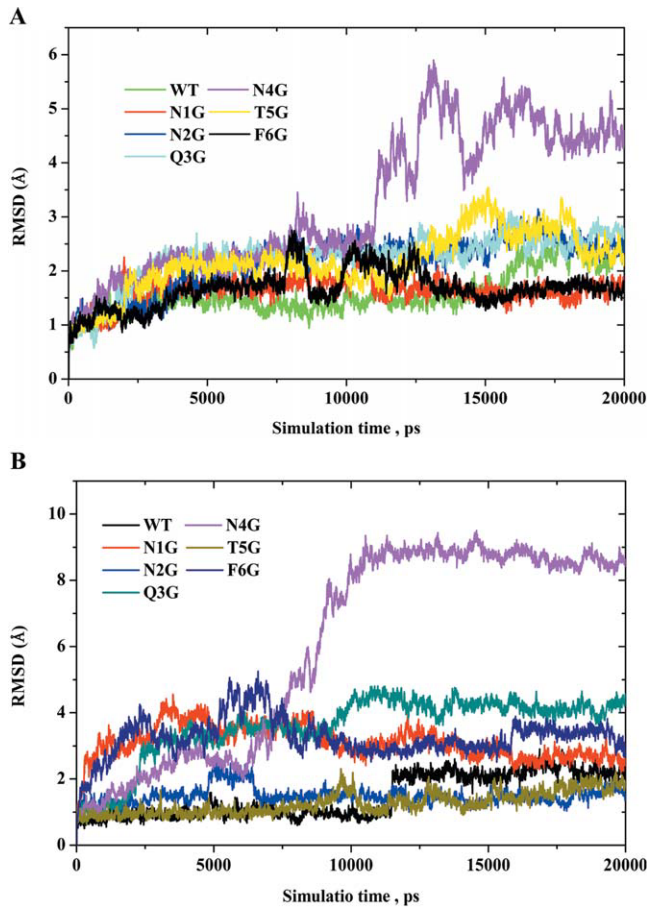


FIGURE 7 Time evolution of the backbone RMSD of the five β -strands double-sheet wild-type elk prion NNQNTF sequence and its mutants. (A) The initial structure is from polymorph I x-ray structure and (B) the initial structure is from polymorph II x-ray structure.

lecular Mechanics-Poisson-Boltzmann/Surface Area) module^{61,62} in the AMBER 11 package. The determination of the binding free energy following the MM-PBSA approach has been described in the past and has been shown to be a good method for comparing binding energies between similar peptides.⁶³ In the MM-PBSA calculation, the dielectric constant of water is set to 80 and no distance cutoff is used. The binding energy between two β -sheets was calculated by

$$\langle \Delta G_{\text{binding}} \rangle = \langle \Delta G_C \rangle - \langle \Delta G_A \rangle - \langle \Delta G_B \rangle \quad (1)$$

where C, A, and B stand for complex (the double-layer sheet) sheet 1 and sheet 2. The free energy of each system X = A, B, or C was computed as a sum of the three terms.^{64,62}

$$\langle \Delta G_X \rangle = \langle E_{\text{MM}} \rangle + \langle \Delta G_{\text{solv}} \rangle - T \langle S \rangle \quad (2)$$

where E_{MM} is the molecular mechanics energy of the molecule expressed as the sum of the internal energy (bonds,

angles, and dihedrals) (E_{int}), electrostatic energy (E_{ele}) and Van Der Waals term (E_{vdw}):

$$E_{\text{MM}} = E_{\text{int}} + E_{\text{ele}} + E_{\text{vdw}} \quad (3)$$

ΔG_{solv} accounts for the solvation energy which can be divided into the polar and nonpolar part:

$$\Delta G_{\text{solv}} = \Delta G_{\text{PB}} + \Delta G_{\text{SA}} \quad (4)$$

The polar part ΔG_{PB} accounts for the electrostatic contribution to solvation and is obtained by solving the linear Poisson-Boltzmann equation in a continuum model of the solvent.

The second term ΔG_{SA} is a nonpolar contribution to solvation free energy that is linearly dependent on the solvent accessible surface area (SASA):

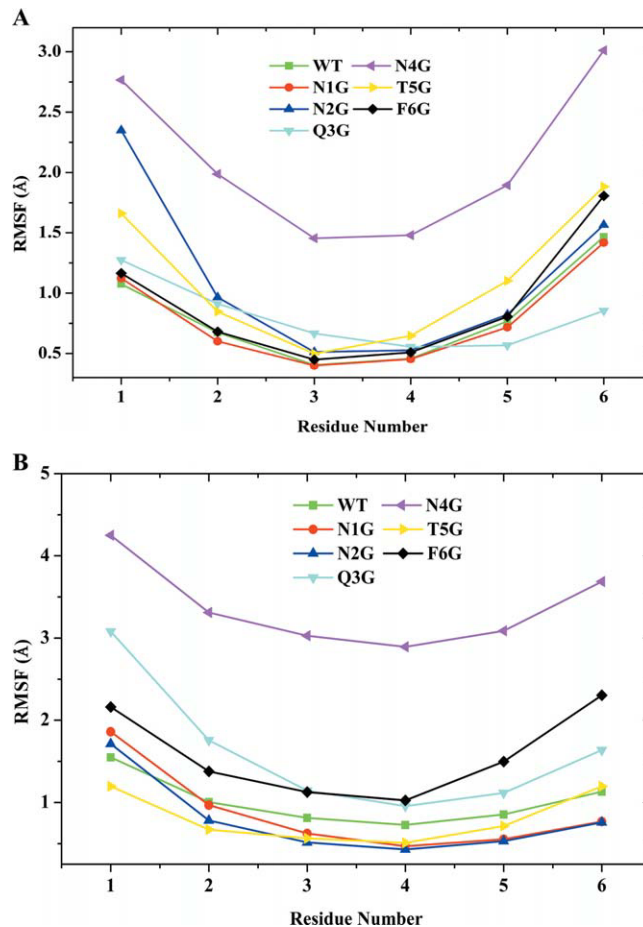


FIGURE 8 Average RMSF values for five β -strands double-sheet wild-type NNQNTF segments of elk prion peptide and its mutant. (A) Wild-type models of NNQNTF polymorph form I and its glycine mutants (B) Wild-type models of NNQNTF polymorph form II and its glycine mutants.

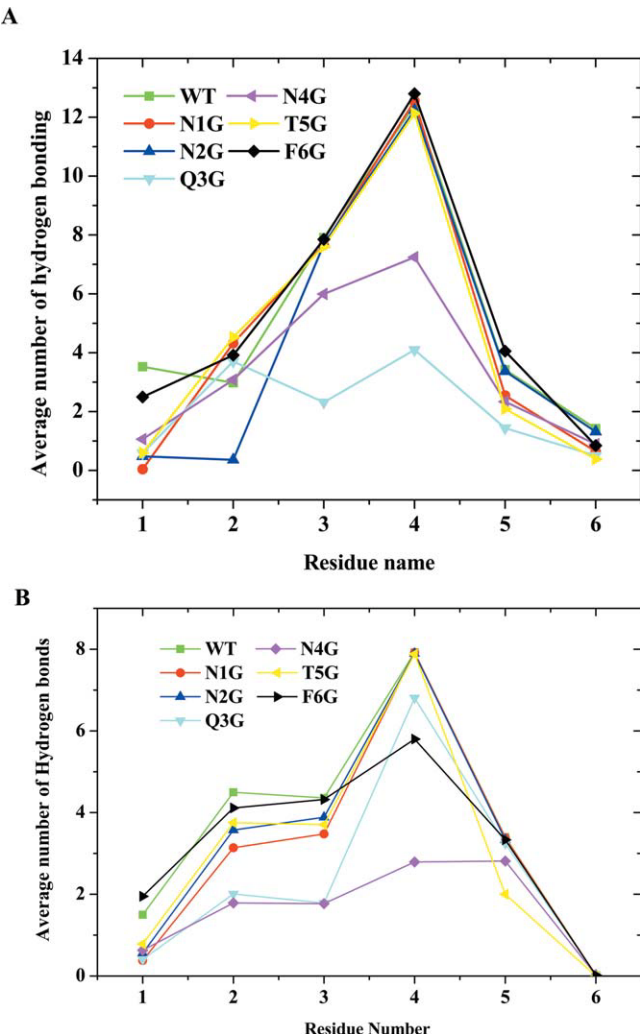


FIGURE 9 Average numbers of hydrogen bonds for individual residues from the simulations of the wild-type models of NNQNTF segment of elk prion and its mutants. (A) Wild-type models of NNQNTF form I and its glycine mutants. (B) Wild-type models of NNQNTF form II and its glycine mutant.

$$\Delta G_{\text{SA}} = \Delta S_{\text{ASA}} + b \quad (5)$$

The ΔG_{SA} was calculated using AMBER11 default parameter for γ and b [Eq. (5)].⁶² The ensemble entropy's contribution to the binding energy of the peptide–peptide interaction is the sum of its translational, rotational, and vibrational entropies:

$$T\langle\Delta S\rangle_{\text{bind}} = T\langle\Delta S\rangle_{\text{tra}} + T\langle\Delta S\rangle_{\text{rot}} + T\langle\Delta S\rangle_{\text{vib}}. \quad (6)$$

The result of the binding energy calculations are shown in Table IV. The sums of the translational and rotational entropies for the double layer with five strands of the wild-type of

NNQNTF from the elk prion and its glycine mutants are around -28 kcal/mol at 300 K irrespective of the peptide sequence structures, which are associated with the conformational restriction of the overall motion upon binding.⁶⁵ Thus, the overall variation of the conformational entropy was determined by the vibrational entropy. Vibrational entropy is the dominant factor that determines the overall entropy penalty for peptide–peptide association.

Detailed characterization of individual energy terms of the calculated binding free energy are shown in Table IV. An inspection of the free energy components for the wild types and mutants investigated in this study reveals that the electrostatic component of the free energy of binding (ΔG_{solv}) contributes unfavorably to binding ($\Delta G > 0$). The nonpolar component G_{SA} contributes favorably ($\Delta G < 0$) as expected, as formation of complexes reduces solvent-accessible surface area. Entropy was found to contribute unfavorably to binding. In most cases, the electrostatic component of the solvation free energy ΔG_{PB} is consistently unfavorable, while ΔG_{ele} , the interaction energy due to electrostatic interaction between sheets, led to favorable binding. These observations are consistent with previous calculations of the electrostatic component of the free energy of solvation.^{62,43} However, the less favorable electrostatics in each case is compensated by the highly favorable nonpolar component of the free energy. In each case, the favorable nature of the nonpolar interaction mostly originates from the van der Waals interaction energy ΔG_{vdW} as opposed to the nonpolar component of solvation ΔG_{SA} . There did not appear to be a clear trend for the entropy change upon binding ($T\Delta S$).

The result of the binding free energy calculation (Table IV) indicates that the structurally stable models have the lowest binding free energy, while the models which are structurally unstable were found to have the largest binding free energy. The wild-type polymorph 1 with a greater number of total hydrogen bonds is a more ordered complex and have a lower binding energy of -36.3 Kcal/mol compared to the wild-type polymorph 2 with less favorable binding energy (-18.7 kcal/mol). The significant difference (ca. -17.8) in binding energy indicates the importance of the interface area and surface complementarity (726 \AA^2 vs. 516 \AA^2 interface area⁸). The difference in binding free energy between the unmutated (wild type) and mutated complex is defined as:

$$\Delta\Delta G_{\text{mut}} = \Delta G_{\text{mut}} - \Delta G_{\text{wild}}$$

A positive and negative $\Delta\Delta G_{\text{mut}}$ values indicate the unfavorable and favorable contributions. The binding energy difference for the mutant N4G (which is structurally unstable) for both polymorphic forms has relatively larger positive values

Table III Summary of Structural Analysis of NNQNTF Aggregate Oligomers from MD Trajectories of the Wild-Type and Single Point Glycine Mutant of the Elk Prion Fragment Form X-ray Structure of Polymorph II

System	RMSD	RMSF	$d_{\text{intersheet}}$	$d_{\text{interstrand}}$	# H bond per strand	Secondary structure	
						β sheet	Turn
2ST-1SH	9.4 ± 7.3	9.9 ± 0.4		10.6 ± 4.3	0.2 ± 0.1	28.4 ± 1.7	71.6 ± 1.7
3ST-1SH	4.9 ± 1.1	3.0 ± 1.1		7.1 ± 0.7	0.8 ± 1.0	87.3 ± 1.7	12.6 ± 1.1
4ST-1SH	6.5 ± 5.9	3.9 ± 1.5		9.2 ± 3.1	1.2 ± 0.9	60.2 ± 3.5	39.8 ± 2.0
5ST-1SH	4.7 ± 1.1	7.0 ± 1.8		6.7 ± 0.4	2.7 ± 2.4	87.8 ± 2.2	12.2 ± 0.9
2ST-2SH	4.2 ± 1.9	2.4 ± 1.2	10.9 ± 1.4	7.6 ± 3.0	0.3 ± 0.1	85.4 ± 3.7	14.6 ± 1.9
3ST-2SH	1.1 ± 0.2	1.0 ± 0.5	9.7 ± 0.2	5.1 ± 0.1	1.1 ± 1.0	99.9 ± 2.4	0.1 ± 0.1
4ST-2SH	2.2 ± 0.3	0.7 ± 0.6	10.6 ± 0.2	5.0 ± 0.1	2.7 ± 1.98	99.5 ± 2.4	1.4 ± 0.4
5ST-2SH	1.5 ± 0.6	0.8 ± 0.6	9.4 ± 0.1	5.1 ± 0.1	3.6 ± 2.73	96.7 ± 3.0	3.2 ± 0.5
N1G	3.1 ± 0.9	0.8 ± 0.5	9.4 ± 0.1	5.3 ± 0.2	3.1 ± 2.8	97.2 ± 3.1	2.9 ± 0.6
N2G	1.5 ± 0.3	0.8 ± 0.5	9.4 ± 0.1	5.0 ± 0.1	3.2 ± 2.8	96.9 ± 3.2	3.1 ± 0.4
Q3G	3.6 ± 0.9	0.8 ± 0.6	11.1 ± 0.6	6.0 ± 0.5	2.4 ± 2.5	92.4 ± 3.9	7.6 ± 1.4
N4G	6.00 ± 3.1	2.1 ± 1.4	11.0 ± 1.6	7.8 ± 1.5	1.6 ± 1.1	92.8 ± 5.2	7.2 ± 1.2
T5G	1.3 ± 0.3	1.1 ± 0.9	9.7 ± 0.3	5.1 ± 0.1	3.0 ± 2.8	94.4 ± 4.2	5.6 ± 0.9
F6G	3.3 ± 0.6	0.9 ± 0.6	9.5 ± 0.2	5.2 ± 0.1	3.0 ± 2.0	92.4 ± 3.2	7.6 ± 1.4

of $\Delta\Delta G_{\text{mut}}$ indicating the unfavorable association of this particular peptide-peptide double layer system. Substitution of N4 by a small, short Gly not only disrupts the steric zipper shape complementary but also weakens hydrophobic interactions between residues N4-N4 (Figure S1 and S2), leading to an increase in packing energy (~ 30 kcal/mol) between the two β -sheets relative to the wild-type interface (Figures S1 and S2). The mutants N1G, Q3G, T5G, and

F6G show negative values with favorable peptide-peptide association for polymorph 1. In the case of polymorph 2, the $\Delta\Delta G_{\text{mut}}$ values were found to be all positive with N4G and Q3G showing the largest positive value and T5G and F6G the smallest. The trend in the calculated binding free energy is in agreement with the observed instability based on RMSD, RMSF, and interstrand and intersheet distance. Those aggregated oligomer models which show structural

Table IV Binding Free Energy of Double Layer with Five Strands of the NNQNTF Segment of Elk Prion and Its Mutants

PDB	Type	ΔE^{elea}	ΔE^{vdw}	$\Delta G_{\text{PB}}^{\text{sol}}$	$\Delta G_{\text{SA}}^{\text{sol}}$	$\Delta G_{\text{subtotal}}^{\text{b}}$	$T\Delta S_{\text{vib}}$	$\langle \Delta G_{\text{wild}} \rangle$	$\langle \Delta G_{\text{mut}} \rangle$	$\langle \Delta\Delta G_{\text{mut}} \rangle^{\text{c}}$
(A) Wild Type of NNQNTF Polymorph Form I and Its Mutants										
3FVA	WT	-115.9 ± 6.5	-917.7 ± 88.2	943.1 ± 84.9	-9.8 ± 0.5	-100.3 ± 11.8	-35.9	-36.3		
	N1G	-106.8 ± 6.6	-1473.4 ± 219.9	1480.2 ± 194.9	-9.3 ± 0.4	-109.3 ± 28.5	-30.2		-51.3	-15
	N2G	-99.2 ± 8.1	-699.4 ± 147.2	731.1 ± 148.5	-8.2 ± 0.8	-75.8 ± 11.5	-38.5		-9.5	26.8
	Q3G	-92.8 ± 6.48	-1367.9 ± 72.5	1372.1 ± 66.9	-10.1 ± 0.4	-98.7 ± 11.7	-29.9		-40.9	-4.6
	N4G	-98.1 ± 9.3	-759.8 ± 98.66	785.9 ± 82.21	-9.1 ± 0.7	-81.1 ± 14.3	-48.2		-4.9	31.4
	T5G	-100.67 ± 6.8	-1254.6 ± 86.8	1244.6 ± 81.2	-9.1 ± 0.4	-119.9 ± 16.6	-33.6		-58.4	-24.8
	F6G	-108.3 ± 6.5	-820.9 ± 75.8	847.2 ± 75.4	-9.0 ± 0.5	-91.1 ± 10.1	-28.0		-35.3	-1.0
(B) Wild Type of NNQNTF Polymorph Form II and Its Mutants										
3FVA	WT	-104.4 ± 4.4	-515.5 ± 39.4	552.5 ± 40.3	-7.9 ± 0.2	-75.4 ± 4.4	-28.7	-18.7		
	N1G	-100.1 ± 5.0	-713.5 ± 66.9	760.4 ± 72.8	-7.6 ± 0.4	-60.8 ± 7.4	-29.7		-3.2	15.5
	N2G	-102.7 ± 4.8	-695.5 ± 71.3	743.4 ± 76.3	-7.69 ± 0.4	-62.5 ± 6.8	-30.8		-3.8	14.9
	Q3G	-80.5 ± 7.9	-388.0 ± 63.2	421.9 ± 63.9	-6.4 ± 0.6	-53.1 ± 8.5	-32.6		7.1	25.8
	N4G	-92.4 ± 10.0	-757.7 ± 85.4	782.2 ± 83.2	-9.1 ± 0.9	-77.0 ± 11.5	-58.5		9.35	28.1
	T5G	-94.2 ± 6.6	-490.1 ± 41.1	524.3 ± 40.7	-7.4 ± 0.4	-67.4 ± 6.7	-22.7		-16.9	1.8
	F6G	-67.6 ± 6.2	-1076.0 ± 121.7	1066.6 ± 110.6	-7.8 ± 0.3	-84.8 ± 16.5	-41.18		-15.9	2.8

^a Units in kcal/mol; ΔE^{elea} , nonsolvent electrostatic potential energy; $\Delta G_{\text{PB}}^{\text{sol}}$, electrostatic contributions to the solvation free energy calculated with Poisson-Boltzmann equation; $G_{\text{SA}}^{\text{sol}}$, nonpolar contributions to solvation free energy; ΔE^{vdw} , van der Waals potential energy; $T\Delta S$, the entropic contribution calculated to the free energy of binding; $\Delta G_{\text{binding}}$, calculated binding free energy, $\Delta\Delta G_{\text{mut}}$, change in free energy induced by mutation.

^b $\Delta G_{\text{binding}} = \Delta G_{\text{subtotal}} - T\Delta S$, Translational and rotational free energies were $-T\Delta S_{\text{trans}} = 14.42$ kcal/mol and $-T\Delta S_{\text{rot}} = 13.55$ kcal/mol, which were subtracted from $\Delta G_{\text{binding}} = \Delta G_{\text{subtotal}} - T\Delta S_{\text{vib}}$ when calculating $\Delta G_{\text{binding}}$. $T\Delta S = T\Delta S_{\text{tra}} + T\Delta S_{\text{rot}} + T\Delta S_{\text{vib}}$.

^c $\Delta\Delta G_{\text{mut}} = \Delta G_{\text{mut}} - \Delta G_{\text{wild}}$, the change of mutant binding free energy as to wild-type.

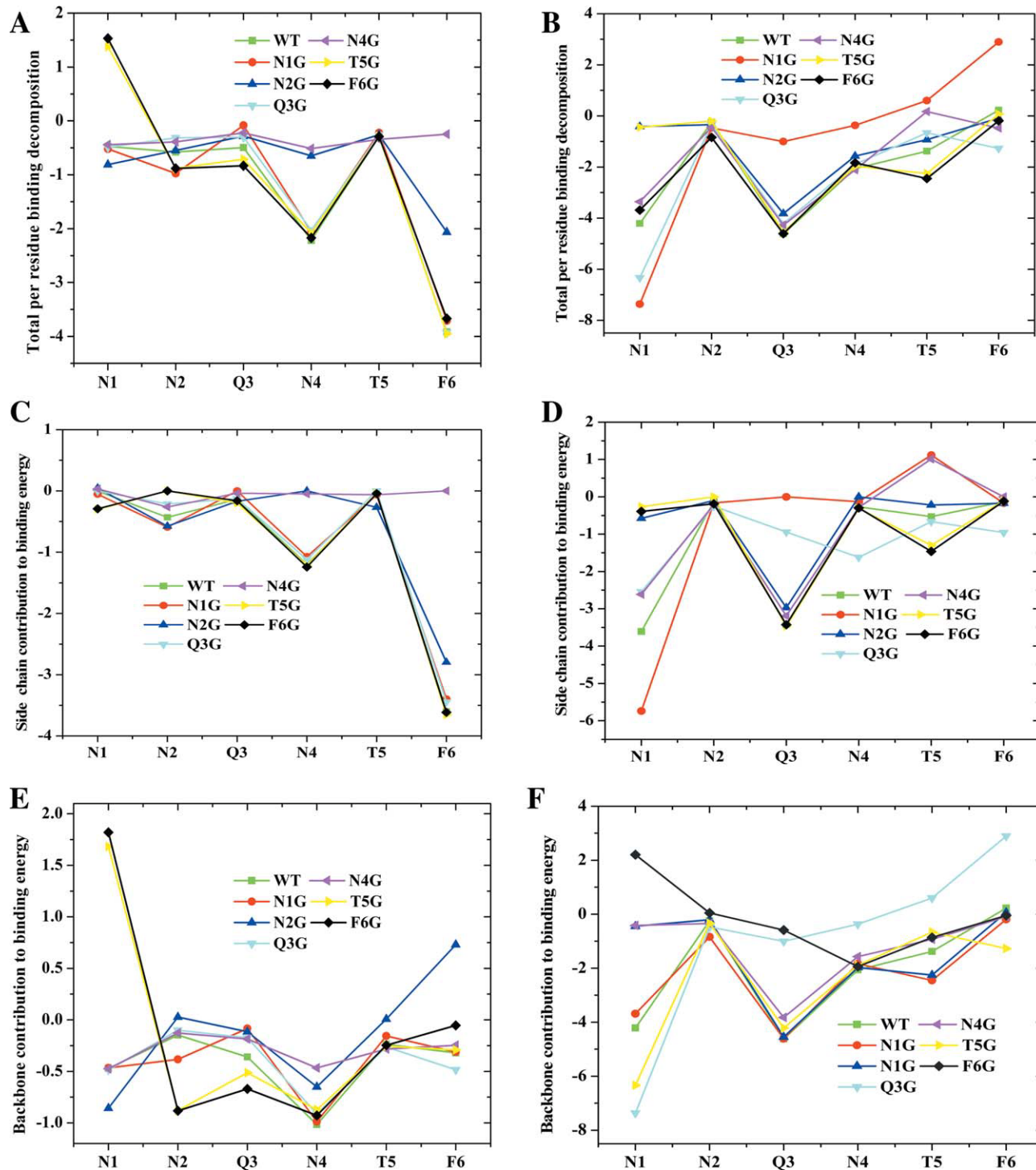


FIGURE 10 MM-PBSA per residue decomposition of the binding free energy of the wild-type and mutants. The energy term corresponds to the sum of backbone and side chain contribution (A and B), side chain (C and D), and backbone (E and F). The results on the right correspond to polymorph 1 and the left to polymorph2. A negative value indicates residue makes favorable contribution.

instability were found to have unfavorable binding energy compared with the stable ones. The disordered mutant oligomers have a greater entropic penalty for binding compared with the wild type. Results from this work provided

valuable insight into the forces that drive the stability of the peptide-peptide complexes of the five-stranded double layer aggregation oligomer models of elk prion and those that lead to unstable complexes. The study of the wild type

and mutants in an explicit solvent will provide valuable insight to guide design efforts in future amyloid aggregation inhibitor.

In order to identify the residues that contribute the most to the calculated overall binding energy, we used a residue-by-residue decomposition protocol embedded in the PB solvent model based in MM-PBSA. Using this model, the calculated energies can be further broken down into individual residue's contributions. Binding free energy decomposition at the atomic level was made to evaluate the contribution of each residue to the total binding free energy, as well as the contributions of its side chain and backbone. As can be seen, the residues making the most favorable contributions to the binding free energy between the two sheets are residues Asn2, Asn4, and Phe6 for polymorph 1 and Asn1, Gln3, and Thr5 (Figure 10). Their contribution to the binding free energy ranges from -0.5 to -4.0 kcal/mol. These residues are situated at the interface between the two sheets and exchange stable hydrogen bonds between their backbone atoms and van der Waals interactions between their side chains. The contribution of the side chains to the association of the five-stranded double layer oligomers is larger than that of the backbone atoms, underlining their importance. Mutation of the side-chains at the interface to the smallest amino acid glycine resulted in the reduced side-chain continuation of the targeted amino acid, and this leads to the total binding free energy of the sheet to sheet association.

It is also worth noting that a "single-trajectory" approach has been used in the literature to study the association free energy.^{24,66} It gave an insight into the role of various energy components on the assembly of the amylin fragment oligomer. The smaller binding free energy of the mutants (N1G and T5G) is due to reduced layer-to-layer distance (intersheet distance) leading to favorable hydrogen-bond geometry (thus enhancing the formation of side-chain hydrogen bonds between the sheets) compared with the wild type making the mutant more advantageous to form a tighter steric zipper (see the intersheet distance in Table S1). This is in agreement with the observation of the sheet-to-sheet interface packing on binding energy observed by Wu et al.⁶⁷ One of the polymorphs (form 1) has an additional intersheet hydrogen bonding (about 10) which contributes significantly to its stability over polymorph 2 (average number of H-bonds of 5.28 ± 4.1 of WT form 1 versus 3.61 ± 2.7 of WT form 2, see Tables S1 and S2). Berryman et al.⁶⁸ have used the average number of H-bonds per monomer to explain the result of the calculated binding free energy from MM-GBSA for the two polymorphic forms of GNNQQNY aggregates. An additional stabilizing factor for polymorph form 1 is the tight hydrophobic interface that stabilizes the

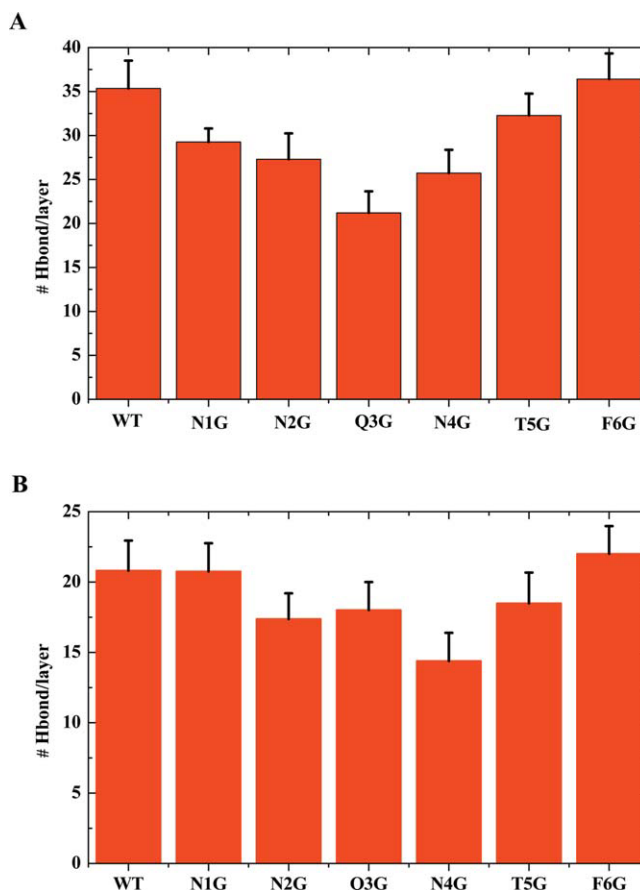


FIGURE 11 Average number of H-bonds per layer: wild-type and mutants of NNQNTF polymorph I (A) and wild-type and mutants of NNQNTF polymorph II (B).

double layer, and this is an additional reason for the predicted small binding energy for polymorph 1.

Our calculation shows that polymorph 1 is the most stable. To investigate the effect of the hydrogen bonds on the ranking of the stability of wild type and mutants we examined the hydrogen bond occupancy⁶⁹ and the average number of hydrogen bonds per β -sheet (Tables S1 and S2 and Figure 11). In order to discriminate between hydrogen bonds that remain intact for most of the trajectory and those which are formed and disrupted more frequently, we considered only those stable hydrogen bonds (defined as present in at least 50% of the analyzed fame).

Hydrogen bond contents of β -sheet double layers were used previously to judge the structural integrity and stability of the various β -sheet aggregates.⁷⁰ We did a similar analysis and we found the binding energy ranking to be supported with the hydrogen bonding occupancy analysis as show in Tables S1 and S2. The highest energy corresponds to the mutants with reduced occupancy of the main chain and the

side chain (especially intersheet hydrogen bonds in polymorph form 1 aggregates), confirming their inability to optimize further the intermolecular distances and interactions. The hydrogen bond analysis in combination with the result of intersheet distance and secondary structure were found to support the ranking of the wild type and mutants stability based on the binding free energy analysis despite the use of the single trajectory approach in our calculation of the free energy.

Several groups have shown that peptides or peptidomimetics can inhibit A β aggregation.³³ Our simulations could be a starting point for designing peptidomimetic inhibitor of the elk prion. The synthetic peptides suffer from a disadvantage of being able to undergo self-amyloidosis, which limits their application in therapeutic development. The strategy of N-methylation of peptide amide bonds has been a well-known protein-design approach to suppress H-bonding ability of an >NH group and to restrict the conformation of the backbone. The identification of amino acid important in stabilizing the amyloid aggregate using MD simulation based on a single point mutation with β -breaker amino acid and combining this with N-methylation of the peptide amide could be a variable option. The designed molecule can prevent fibrils from forming, and break down pre-formed fibrils.⁷¹

CONCLUSIONS

In this work, we explore the effect of β -sheet-to- β -sheet organization on the structure, dynamics, and association of NNQNTF segment of the elk prion aggregation oligomers in solution using MD simulations. Our results show that the structural stability of the NNQNTF oligomers increases with increasing the number of β -strands for double layers. We further proposed that the octameric structure (the SH2-ST4 model in this study) is the possible nucleus seed for NNQNTF protofibril formation. Designed mutants with substituted residues occurring at the interfaces (especially Asn4) display lower structural stability. Our results also demonstrated that hydrophobic interaction is the principle driving force to stabilize the adjacent β -strands while the steric zipper is responsible for holding the neighboring β -sheet layers together. We used free energy calculations following the MM-PBSA approach to determine the role of nonpolar effects, electrostatics, and entropy in binding. Nonpolar effects remained consistently more favorable in wild type and mutants five-stranded double layer aggregate models, reinforcing the importance of hydrophobic effects in protein-protein binding. While entropy systematically opposed binding in all cases, there was no observed trend in the entropy difference between wild-type and glycine mutant. A per-atom decomposition of the binding free

energy has been performed to identify the residues contributing most to the self-association free energy. Residues that are situated at the interface between the two sheets were found to make favorable contributions to the peptide-peptide association. Results from this work provided valuable insight into the aggregation of the NNQNTF peptide and the forces that drive peptide-peptide complexes. The study of the wild type and mutants in explicit solvent may provide valuable insight to guiding future amyloid aggregation inhibitor design efforts.

This research used resources of the National Energy Research Scientific Computing Center, which is supported by the Office of Science of the U.S. Department of Energy under contract no. DE-AC02-05CH11231. We thank Dr. Michael R. Sawaya for providing the structure of the small β -cross polymorphic models. This work was supported in part by the National Science Foundation (CCF/CHE 0832622).

REFERENCES

1. Serpell, L. C.; Sunde, M.; Blake, C. C. F. *Cell Mol Life Sci* 1997, 53, 871–887.
2. Sawaya, M. R.; Sambashivan, S.; Nelson, R.; Ivanova, M. I.; Sievers, S. A.; Apostol, M. I.; Thompson, M. J.; Balbirnie, M.; Wiltzius, J. J. W.; McFarlane, H. T.; Madsen, A. O.; Riek, C.; Eisenberg, D. *Nature* 2007, 447, 453–457.
3. Luca, S.; Yau, W. M.; Leapman, R.; Tycko, R. *Biochemistry* 2007, 46, 13505–13522.
4. Zheng, J.; Jang, H.; Ma, B.; Tsai, C. J.; Nussinov, R. *Biophys J* 2007, 93, 3046–3057.
5. Fandrich, M.; Meinhardt, J.; Grigorjeff, N. *Prion* 2009, 3, 89–93.
6. Miller, Y.; Ma, B.; Nussinov, R. *Chem Rev* 110, 4820–4838.
7. Wiltzius, J. J. W.; Sievers, S. A.; Sawaya, M. R.; Cascio, D.; Popov, D.; Riek, C.; Eisenberg, D. *Protein Sci* 2008, 17, 1467–1474.
8. Wiltzius, J. J. W.; Landau, M.; Nelson, R.; Sawaya, M. R.; Apostol, M. I.; Goldschmidt, L.; Soriaga, A. B.; Cascio, D.; Rajashankar, K.; Eisenberg, D. *Nat Struct Mol Biol* 2009, 16, 973–U998.
9. Teng, P. K.; Eisenberg, D. *Protein Eng Des Sel* 2009, 22, 531–536.
10. Park, J.; Kahng, B.; Hwang, W. *PLoS Comput Biol* 2009, 5, 17.
11. Petkova, A. T.; Leapman, R. D.; Guo, Z. H.; Yau, W. M.; Mattson, M. P.; Tycko, R. *Science* 2005, 307, 262–265.
12. Andersen, C. B.; Hicks, M. R.; Vetri, V.; Vandahl, B.; Rahbek-Nielsen, H.; Thogersen, H.; Thogersen, I. B.; Enghild, J. J.; Serpell, L. C.; Rischel, C.; Otzen, D. E. *J Mol Biol* 397, 932–946.
13. DeMarco, M. L.; Daggett, V. *Proc Natl Acad Sci USA* 2004, 101, 2293–2298.
14. Wu, C.; Lei, H. X.; Duan, Y. *J Am Chem Soc* 2005, 127, 13530–13537.
15. Gnanakaran, S.; Nussinov, R.; Garcia, A. E. *J Am Chem Soc* 2006, 128, 2158–2159.
16. Nguyen, H. D.; Hall, C. K. *Proc Natl Acad Sci USA* 2004, 101, 16180–16185.

17. Zheng, J.; Jang, H.; Nussinov, R. *Biochemistry* 2008, 47, 2497–2509.
18. Masman, M. F.; Eisel, U. L. M.; Csizmadia, I. G.; Penke, B.; Enriz, R. D.; Marrink, S. J.; Luiten, P. G. M. *J Phys Chem B* 2009, 113, 11710–11719.
19. Kent, A.; Jha, A. K.; Fitzgerald, J. E.; Freed, K. F. *J Phys Chem B* 2008, 112, 6175–6186.
20. Zheng, J.; Ma, B. Y.; Chang, Y.; Nussinov, R. *Front Biosci* 2008, 13, 3919–3930.
21. Sgourakis, N. G.; Yan, Y. L.; McCallum, S. A.; Wang, C. Y.; Garcia, A. E. *J Mol Biol* 2007, 368, 1448–1457.
22. Chang, L. K.; Zhao, J. H.; Liu, H. L.; Liu, K. T.; Chen, J. T.; Tsai, W. B.; Ho, Y. *J Biomol Struct Dynam* 2009, 26, 731–740.
23. Zhang, Z. Q.; Chen, H.; Bai, H. J.; Lai, L. H. *Biophys J* 2007, 93, 1484–1492.
24. Xu, W. X.; Ping, J.; Li, W. F.; Mu, Y. G. *J Chem Phys* 2009, 130, 8.
25. Kayed, R.; Pensalfini, A.; Margol, L.; Sokolov, Y.; Sarsoza, F.; Head, E.; Hall, J.; Glabe, C. *J Biol Chem* 2009, 284, 4230–4237.
26. Quist, A.; Doudevski, L.; Lin, H.; Azimova, R.; Ng, D.; Frangione, B.; Kagan, B.; Ghiso, J.; Lal, R. *Proc Natl Acad Sci USA* 2005, 102, 10427–10432.
27. Vitagliano, L.; Stanzione, F.; De Simone, A.; Esposito, L. *Biopolymers* 2009, 91, 1161–1171.
28. Kayed, R.; Head, E.; Thompson, J. L.; McIntire, T. M.; Milton, S. C.; Cotman, C. W.; Glabe, C. G. *Science* 2003, 300, 486–489.
29. Aguzzi, A.; Sigurdson, C.; Heikenwaelder, M. *Annu Rev Pathol Mech Dis* 2008, 3, 11–40.
30. Wille, H.; Bian, W.; McDonald, M.; Kendall, A.; Colby, D. W.; Bloch, L.; Ollesch, J.; Borovinskiy, A. L.; Cohen, F. E.; Prusiner, S. B.; Stubbs, G. *Proc Natl Acad Sci USA* 2009, 106, 16990–16995.
31. Nguyen, J. T.; Inouye, H.; Baldwin, M. A.; Fletterick, R. J.; Cohen, F. E.; Prusiner, S. B.; Kirschner, D. A. *J Mol Biol* 1995, 252, 412–422.
32. Tanaka, M.; Collins, S. R.; Toyama, B. H.; Weissman, J. S. *Nature* 2006, 442, 585–589.
33. Patino, M. M.; Liu, J. J.; Glover, J. R.; Lindquist, S. *Science* 1996, 273, 622–626.
34. Glover, J. R.; Kowal, A. S.; Schirmer, E. C.; Patino, M. M.; Liu, J. J.; Lindquist, S. *Cell* 1997, 89, 811–819.
35. King, C. Y.; Diaz-Avalos, R. *Nature* 2004, 428, 319–323.
36. Nelson, R.; Sawaya, M. R.; Balbirnie, M.; Madsen, A. O.; Riek, C.; Grothe, R.; Eisenberg, D. *Nature* 2005, 435, 773–778.
37. Ivanova, M. I.; Sievers, S. A.; Sawaya, M. R.; Wall, J. S.; Eisenberg, D. *Proc Natl Acad Sci USA* 2009, 106, 18990–18995.
38. Goldschmidt, L.; Teng, P. K.; Riek, R.; Eisenberg, D. *Proc Natl Acad Sci USA* 2010, 107, 3487–3492.
39. Hall, D.; Edskes, H. *J Mol Biol* 2004, 336, 775–786.
40. Aguzzi, A.; O'Connor, T. *Nat Rev Drug Discov* 2010, 9, 237–248.
41. Stefani, M. *Curr Prot Pept Sci* 2010, 11, 343–354.
42. Wang, W.; Kollman, P. A. *J Mol Biol* 2000, 303, 567–582.
43. Gohlke, H.; Kiel, C.; Case, D. A. *J Mol Biol* 2003, 330, 891–913.
44. Zoete, V.; Meuwly, M.; Karplus, M. *Prot Struct Funct Bioinform* 2005, 61, 79–93.
45. Case, D. A.; Tad Tec, I.; Simmerling, C. L.; Wang, J.; Duke, R. E.; Luo, R.; Crowley, M.; Walker, R. C.; Zhang, W.; Merz, K. M.; Wang, B.; Hayik, S.; Roitberg, A.; Seabra, G.; Kolossváry, I.; Wong, K. F.; Paesani, F.; Vanicek, J.; Wu, X.; Brozell, S. R.; Steinbrecher, T.; Gohlke, H.; Yang, L.; Tan, C.; Mongan, J.; Hornak, V.; Cui, G.; Mathews, D. H.; Seetin, M. G.; Sagui, C.; Babin, V.; Kollman, P. A. University of California San Francisco: San Francisco, 2010.
46. Darden, T.; York, D.; Pedersen, L. *J Chem Phys* 1993, 98, 10089–10092.
47. Ryckaert, J. P.; Ciccotti, G.; Berendsen, H. J. C. *J Comput Phys* 1977, 23, 327–341.
48. Humphrey, W.; Dalke, A.; Schulten, K. *J Mol Graph* 1996, 14, 33–38.
49. Fabiola, F.; Bertram, R.; Korostelev, A.; Chapman, M. S. *Protein Sci* 2002, 11, 1415–1423.
50. Tatarek-Nossol, M.; Yan, L. M.; Schmauder, A.; Tenidis, K.; Westermark, G.; Kapurniotu, A. *Chem Biol* 2005, 12, 797–809.
51. Williams, A. D.; Portelius, E.; Kheterpal, I.; Guo, J. T.; Cook, K. D.; Xu, Y.; Wetzel, R. *J Mol Biol* 2004, 335, 833–842.
52. Tzotzos, S.; Doig, A. J. *Protein Sci* 2010, 19, 327–348.
53. Esposito, L.; Pedone, C.; Vitagliano, L. *Proc Natl Acad Sci USA* 2006, 103, 11533–11538.
54. Buchete, N. V.; Hummer, G. *Biophys J* 2007, 92, 3032–3039.
55. Huet, A.; Derreumaux, P. *Biophys J* 2006, 91, 3829–3840.
56. Zheng, J.; Ma, B. Y.; Tsai, C. J.; Nussinov, R. *Biophys J* 2006, 91, 824–833.
57. Pace, C. N. *Nat Struct Mol Biol* 2009, 16, 681–682.
58. Zanuy, D.; Porat, Y.; Gazit, E.; Nussinov, R. *Structure* 2004, 12, 439–455.
59. Ono, K.; Condron, M. M.; Teplow, D. B. *Proc Natl Acad Sci USA* 2009, 106, 14745–14750.
60. Horn, A. H. C.; Sticht, H. *J Phys Chem B* 114, 2219–2226.
61. Kollman, P. A.; Massova, I.; Reyes, C.; Kuhn, B.; Huo, S. H.; Chong, L.; Lee, M.; Lee, T.; Duan, Y.; Wang, W.; Donini, O.; Cieplak, P.; Srinivasan, J.; Case, D. A.; Cheatham, T. E. *Acc Chem Res* 2000, 33, 889–897.
62. Massova, I.; Kollman, P. A. *J Am Chem Soc* 1999, 121, 8133–8143.
63. Campanera, J. M.; Pouplana, R. *Molecules* 2010, 15, 2730–2748.
64. Chong, L. T.; Duan, Y.; Wang, L.; Massova, I.; Kollman, P. A. *Proc Natl Acad Sci USA* 1999, 96, 14330–14335.
65. Williams, D. H.; Stephens, E.; O'Brien, D. P.; Zhou, M. *Angew Chem Int Ed* 2004, 43, 6596–6616.
66. Jiang, P.; Xu, W. X.; Mu, Y. G. *PLoS Comput Biol* 2009, 5, 13.
67. Wu, C.; Bowers, M. T.; Shea, J. E. *PLoS Comput Biol* 2010, 6, e1000693.
68. Berryman, J. T.; Radford, S. E.; Harris, S. A. *Biophys J* 2009, 97, 1–11.
69. Kieseritzky, G.; Morra, G.; Knapp, E. W. *J Biol Inorg Chem* 2006, 11, 26–40.
70. Zhao, W. H.; Zheng, B.; Haynie, D. T. *Langmuir* 2006, 22, 6668–6675.
71. Amijee, H.; Madine, J.; Middleton, D. A.; Doig, A. J. *Biochem Soc Trans* 2009, 37, 692–696.

Reviewing Editor: David A. Case